Published in final edited form as:

Stroke. 2022 July ; 53(7): 2369–2376. doi:10.1161/STROKEAHA.121.037358.

Rho-kinase inhibition improves the outcome of focal subcortical white matter lesions

Sanem Aykan, MD PhD[1], **Hongyu Xie, MD PhD**[1,2], **Yi Zheng, PhD**[1], **David Y. Chung, MD PhD**[1], **Sreekanth Kura**[4], **James Han Lai**[1], **Taylan D. Erdogan**[1], **Andreia Morais, PhD**[1], **Isra Tamim**[1], **Damla Yagmur, MD**[1], **Hidehiro Ishikawa, MD PhD**[3], **Ken Arai, PhD**[3], **M. Abbas Yaseen, PhD**[6], **David A. Boas, PhD**[4,5], **Sava Sakadzic, PhD**[5], **Cenk Ayata, MD PhD**[1,6]

[1]Neurovascular Research Unit, Department of Radiology, Massachusetts General Hospital, Harvard Medical School, Charlestown, USA

[2]Department of Rehabilitation, Huashan Hospital, Fudan University, Shanghai, China

[3]Neuroprotection Research Laboratory, Department of Radiology and Neurology, Massachusetts General Hospital, Harvard Medical School, Charlestown, USA

[4]Neurophotonics Center, Department of Biomedical Engineering, Boston University, Boston, MA, USA

[5]Athinoula A. Martinos Center for Biomedical Imaging, Department of Radiology, Massachusetts General Hospital, Charlestown, MA, USA

[6]Stroke Service, Department of Neurology, Massachusetts General Hospital, Boston, MA, USA

Abstract

Background: Subcortical white matter lesions are exceedingly common cerebral small vessel disease and lead to significant cumulative disability without an available treatment. Here, we tested a rho-kinase inhibitor on functional recovery after focal white matter injury.

Methods: A focal corpus callosum lesion was induced by stereotactic injection of N^5-(1-iminoethyl)-L-ornithine in mice. Fasudil (10 mg/kg) or vehicle was administered daily for two weeks, starting one day after lesion induction. Resting-state functional connectivity and grid walk performance were studied longitudinally, and lesion volumes were determined at one month.

Results: Resting-state interhemispheric functional connectivity significantly recovered between days 1 and 14 in the fasudil group ($p<0.001$), despite worse initial connectivity loss than vehicle before treatment onset. Grid walk test revealed an increased number of foot faults in the vehicle group compared to baseline, which persisted for at least four weeks. In contrast, the fasudil arm did not show an increase in foot faults and had smaller lesions at four weeks. Immunohistochemical examination of reactive astrocytosis, synaptic density, and mature oligodendrocytes did not reveal a significant difference between treatment arms.

[*]**Corresponding Author:** Cenk Ayata, M.D., Ph.D., Massachusetts General Hospital, 149 13th Street, 6403, Charlestown, MA 02129, USA, Phone: (617) 726-0821; Fax: (617) 726-2547; cayata@mgh.harvard.edu.

CONFLICT(S)-OF-INTEREST/DISCLOSURE(S)

Dr Ayata is on the scientific advisory board of Neurelis, Inc. and serves as a consultant.

Conclusion: These data show that delayed fasudil post-treatment improves functional outcomes after a focal subcortical white matter lesion in mice. Future work will aim to elucidate the mechanisms.

Graphical Abstract

(A) Experimental timeline. RSFC: resting state functional connectivity. L-NIO: N5-(1-Iminoethyl)-L-ornithine dihydrochloride (B) Representative corpus callosum lesion on a coronal section stained by H&E and the field of view for RSFC. (C) Representative interhemispheric RSFC maps and group averaged interhemispheric correlation coefficients along the anteroposterior axis in vehicle or fasudil arms on days 1 and 14 after L-NIO injection in corpus callosum. (D) Number of foot faults in right and left limbs in grid walk test examined longitudinally.

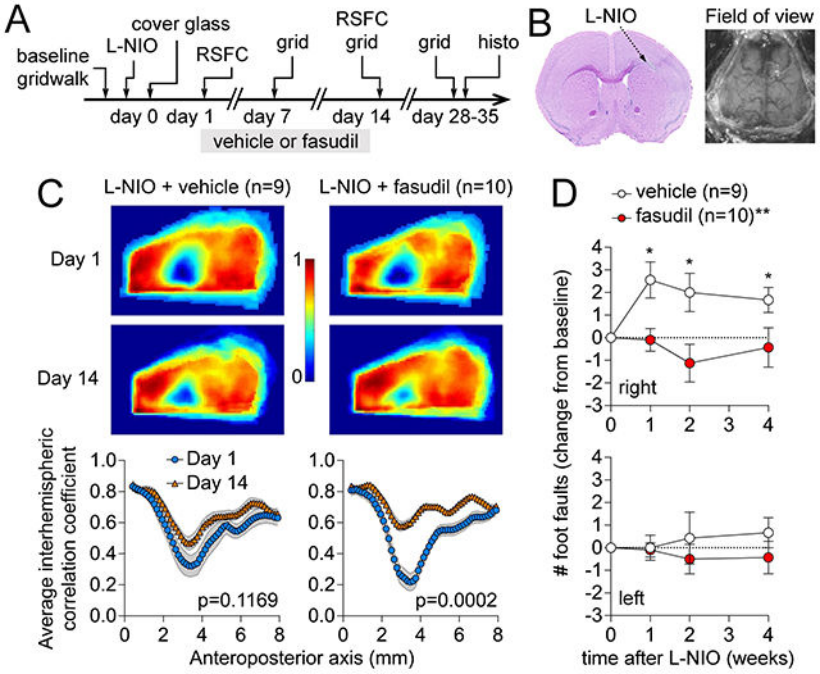

Keywords

animal models; fasudil; optical imaging; resting-state functional connectivity; white matter injury

INTRODUCTION

Subcortical white matter is a common site for small, lacunar-like strokes and leukoaraiosis, often in the setting of cerebral small vessel disease.[1,2] Moreover, traumatic diffuse axonal injury also affects subcortical white matter and the corpus callosum.[3] Although functional consequences of individual white matter lesions can be subtle,[4] cumulative injury can lead to significant disability,[5–7] in part due to loss of interhemispheric connectivity.[8] Prevention is the mainstay for white matter injury as there is no specific treatment to improve the outcomes.

Rho-associated kinase (ROCK) is a crucial regulator of numerous processes in virtually all cells.[9] ROCK inhibitors have been found beneficial in the hyperacute treatment of central nervous system injury.[10] ROCK inhibition promotes axon outgrowth and regeneration,[11,12] and oligodendrocyte precursor cell differentiation and remyelination.[13–15] Indeed, ROCK inhibitors have been shown to augment functional recovery after injury involving long white matter tracts, such as spinal cord injury, large hemispheric ischemic stroke, and cerebral trauma.[10,16–19] We, therefore, hypothesized that ROCK inhibition can improve recovery after a subcortical white matter lesion. Here, we examined the effect of fasudil, an isoform non-selective ROCK inhibitor, on the recovery of resting-state functional connectivity (RSFC) after a small strategically placed lesion in the corpus callosum (CC) in mice,[20] corresponding to the corona radiata in the human brain.

MATERIALS AND METHODS

The data that support the findings of this study are available from the corresponding author upon reasonable request.

Animals

Experiments were approved by the MGH Institutional Animal Care and Use Committee and carried out per the Guide for Care and Use of Laboratory Animals (NIH Publication No. 85-23, 1996). Mice (8-10 weeks old, only males used to avoid confounding effects of estrus cycle, C57BL/6J, Charles River Laboratories), housed on a 12-hour light/dark cycle and fed *ad libitum*, were randomly allocated to study arms, and the procedures and data analyses were carried out in a blinded fashion. The experimental timeline is shown in Figure 1A.

Surgical procedures

A focal CC lesion was induced as previously described with modifications.[20] Briefly, isoflurane-anesthetized mice (4% for induction, 1-1.5% for maintenance, in a 7:3 N_2O:O_2 mixture) were placed on a stereotactic frame (Stoelting, Wood Dale, IL). Rectal temperature was controlled at 37°C by a feedback-regulated homeothermic blanket (FHC, Bowdoin, ME). Ointment was applied to prevent corneal drying. After a midline incision, the scalp was reflected, preserving the periosteum. A burr hole (~1 mm diameter) was drilled under saline cooling centered at 1 mm anterior from bregma adjacent to midline over the right hemisphere. Lesions were induced by stereotactic microinjections of endothelial nitric oxide synthase inhibitor N^5-(1-Iminoethyl)-L-ornithine dihydrochloride (L-NIO; 100 mM, Tocris, Bristol, UK; n=19) using a 5 μL syringe (34G, Hamilton, Reno, NV) connected to an infusion pump (310 Syringe Pump, KD Scientific, Holliston, MA). Two separate injections of 1.2 μL of L-NIO (0.24 μmoles) were performed at a rate of 0.1 μL/minute at 1.5 mm lateral, 1.5 mm anterior, 1.8 mm ventral, and at 1.4 mm lateral, 0.5 mm anterior, 1.6 mm ventral from bregma. To reach these coordinates, the injection needle was inserted at 1.5 and 0.5 mm anterior and 0.2 mm lateral over the dorsal surface and advanced for 2.2 mm and 2.0 mm, respectively, for each injection. To minimize injury to the cortex overlying the lesion, injection needle was inserted adjacent to midline and angled at 36°, pointing laterally (Figure 1B). This approach preserved the skull directly overlying the lesion for imaging purposes. After each injection, the needle was left in place for 5 minutes to avoid backflow,

the absence of which was visually confirmed. After the needle removal, the burr hole was filled with agarose gel. A 12 mm slide cover glass was cut to fit the dorsal skull outline and affixed on the skull using a thin layer of clear cement underneath (Figure 1C). Care was taken to avoid contact between the cement and the cortex. Mice were then placed in a 28 °C incubator for 2 hours before returning to the home cage. In addition to the treatment arms in lesioned mice, we studied naïve mice with identical skull preparation but no needle insertion to demonstrate normal connectivity values on maps and along the anteroposterior axis.

Optical RSFC imaging

To examine RSFC longitudinally in the same animal, we employed intrinsic optical signal imaging of cortical blood volume changes, analogous to brain oxygen level-dependent functional MRI, as previously reported in the normal and injured brain.[20–26] The method relies on resting-state activity-induced changes in blood volume and their temporal correlation to infer connectivity. The experimental setup and analysis have been previously described with modifications.[20] Animals were anesthetized using 2,2,2-tribromoethanol (TBE), also known as Avertin. The solution was prepared protected from light by mixing 0.5 mL stock solution (10 g 2,2,2-tribromoethanol in 6.25 mL tert-amyl alcohol; Sigma-Aldrich, T48402-25G, and Fisher Scientific, A730-1, respectively) with 39.5 mL 0.9% normal saline, stored at 4°C for no longer than one month. Anesthesia was induced by 0.4 mL intraperitoneal dose and maintained with 0.1 ml every 8 minutes. We have previously shown this anesthetic regimen to be superior for RSFC imaging.[23] Animal was then placed on a homeothermic heating pad to maintain the rectal temperature at 37.0±0.1°C and the head was fixed in a stereotaxic frame.

The skull was exposed after a midline incision without damaging the periosteum. Skull surface was illuminated by a quartz tungsten halogen lamp (Techniquip R150, Capra Optical, Natick, MA), passed through a 570±10 nm filter, and directed with a fiberoptic cable to image changes in total hemoglobin concentration (i.e., blood volume). RSFC imaging using a single 570 nm wavelength centered at the isosbestic point between deoxy- and oxyhemoglobin has been validated.[27] Images were acquired with a CCD camera (Cascade 512F, Photometrics, Tucson, AZ) at 256x256 pixel resolution (2x2 binning) and 13.6 frames per second for 10 minutes. μManager software was used for image acquisition (San Francisco, CA). Images were processed, and correlation coefficients were generated as previously described.[23,27,28] In brief, acquired images were downsampled to 128x128 pixels using custom scripts (MATLAB, MathWorks, Natick, MA). The dynamic optical density at each pixel over time was bandpass filtered between 0.008 Hz and 0.09 Hz, downsampled to 1 frame/second, and regressed to remove any global signal variance. *Interhemispheric homotopic connectivity* maps were generated by calculating the correlation coefficients between each pixel and its mirror pixel over the contralateral cortex. The average coronal interhemispheric homotopic correlation coefficients were plotted along the anteroposterior axis. *Seeds* were placed over the secondary motor cortex, the whisker barrel cortex, the visual cortex, and the cortex overlying the corpus callosum lesion, on the ipsilesional hemisphere and the homotopic regions in the contralesional hemisphere, guided by an overlaid atlas.[29] The correlation coefficients between manually placed seeds and all other pixels were calculated and mapped throughout the image to create seed-based connectivity

maps. A correlation matrix was generated between each pair of seeds. All scripts are available from the authors upon reasonable request.

Treatment

Fasudil HCl (Selleck Chemicals, Houston, TX) was dissolved in 0.9% NaCl at a concentration of 2 mg/ml and administered at a dose of 10 mg/kg based on previous work in mice. Vehicle or fasudil treatment started on day one right after the first RSFC imaging, and continued for two weeks twice a day in a blinded fashion (Figure 1A).

Neurological exam

Grid walk test was used to evaluate motor coordination at baseline (i.e., pre-lesion) and 1, 2, and 4 weeks after the lesion.[30] We chose this test because, in our previous work examining neurological deficits after similar subcortical white matter lesions, we found the grid walk test to be marginally superior and sensitive compared with the other tests.[31,32] Mice were placed on a wire grid (1.5 cm square opening) and allowed to walk for 100 steps freely. The total number of forelimb foot faults (per 100 steps) was counted and expressed as a change from the pre-lesion baseline.

Histology and immunohistochemistry

After the last neurological test, brains were harvested and fresh frozen using methylbutane, coronal cryosectioned (20 μm-thick slices, every 200 μm), and stained with hematoxylin and eosin. Images were digitized (Super Coolscan 9000 ED Scanner, Nikon), and lesion area and the distance of lateral and medial lesion boundaries from the midline at each coronal section were measured (ImageJ, NIH, Bethesda, MD). Parallel sections were immunostained for glial fibrillary acidic protein (GFAP), synaptophysin, glutathione S-transferase pi (GST-pi), and 4′,6-diamidino-2-phenylindole (DAPI). Briefly, sections were dried under a fan for 20 minutes, fixed in 4% paraformaldehyde in 1x phosphate-buffered saline (PBS)for 20 minutes, and rinsed three times in 1x PBS for 10 minutes each wash. Tissue sections were then blocked for 1 hour at room temperature in either 1x PBS containing 5% donkey normal serum (Jackson ImmunoResearch Laboratories, West Grove, PA, USA) and 0.1% triton x-100 (Sigma Aldrich, St. Louis, MO, USA) for synaptophysin staining or 3% bovine serum albumin in PBS for GST-pi staining. Blocking solution was decanted off sections, and tissues were incubated in 1x PBS containing 3% donkey normal serum, monoclonal rabbit anti-human synaptophysin antibody (Abcam, Waltham, MA, USA), or rabbit anti-Human GST-pi antibody (1:100; MBL) at 1:100 dilution overnight at 4 degrees Celsius. The following morning, tissue sections were washed 3 times in 1x PBS for 10 minutes per wash, and tissues were incubated in 1x PBS containing 3% donkey normal serum, Cy3 conjugated monoclonal anti-mouse GFAP antibody (Sigma Aldrich, St. Louis, MO, USA) at 1:1000 dilution, Alexa 488 conjugated anti-rabbit IgG antibody (Invitrogen, Waltham, MA, USA) at 1:300 dilution, and DAPI (Roche Diagnostics, Indianapolis, IN, USA) at 1 ug/mL for 1 hour at room temperature. The slides were then washed in 1x PBS 3 times for 10 minutes per wash and coverslipped with Fluoromount-G (Electron Microscopy Services, Hatfield, PA, USA).

Images of coronal sections were taken at 4x and 10x magnification (E-800 microscope, pco.panda sCMOS camera, Nikon, Japan). Images were taken at 5 section levels at 200-μm intervals centered on the lesion along its anteroposterior axis. Acquisition settings were fixed for all sections and brains. For double and triple labeling, the images were acquired sequentially in the same field and merged in ImageJ (NIH, USA). GFAP staining intensity was quantified using 10x magnification with the field centered on the lesion or the same region in the contralateral hemisphere. Mean gray values of all pixels in the field of view were calculated after excluding staining artifacts by hand. Synaptophysin staining intensity was quantified in 4x magnification in a region of interest (ROI) encompassing the cortex but excluding the corpus callosum and the lesion and the same region in the contralateral hemisphere. Mean gray values of all pixels inside the ROI were then measured. Ventricles and negative space in the images were excluded from all measurements. To assess the mature oligodendrocytes in the corpus callosum, we used merged images for GST-pi and DAPI. The number of GST-pi positive cells was counted in a square region of interest (0.0625 mm^2) placed in the center of the median corpus callosum at the section level in the middle of the lesion along its anteroposterior axis. Positive cells were identified by GST-pi staining along with DAPI nuclear stain as previously described.[33]

Statistics

In the absence of prior experience, the sample size was selected empirically to achieve 80% power to detect a 40% effect size, assuming a standard deviation of 30% of the mean interhemispheric homotopic connectivity (α=0.05). Mice were randomly picked from the cages and assigned to treatment arms; no specific randomization tool was used. Data analysis was performed blinded. A priori exclusion criteria included surgical complications (n=1 in the vehicle arm). Statistical comparisons were designed, *a priori*, to compare pre- vs. post-treatment connectivity within each study arm using two-way ANOVA for repeated measures, followed by Sidak's multiple comparisons (Prism 8, GraphPad Software, Inc., CA, USA). Normal distribution was tested by the Shapiro-Wilk test. Data are shown as mean ± SEM.

RESULTS

The chronic cover glass model provided an excellent field of view for interhemispheric RSFC calculation between mirror pixels (Figure 2A). In animals with skull preparation only (n=4), we found strong interhemispheric connectivity when displayed either as an average correlation coefficient map (Figure 2A, upper right panel) or as the average correlation coefficients along the anteroposterior axis (Figure 2A, lower right panel). The CC lesion resulted in the loss of interhemispheric connectivity on day 1, which was most conspicuous overlying the lesion extending laterally (Figure 2B). In vehicle-treated mice (n=9), the interhemispheric connectivity did not significantly improve over the next two weeks (Figure 2B, left). In contrast, fasudil treatment between days 1 and 14 resulted in substantial recovery of connectivity over 2 weeks (n=10), despite somewhat worse deficit on day 1 compared with the vehicle group (Figure 2B, right). Further exploratory spatial analysis using seeds did not reveal a conspicuous regional predilection for recovery (Figure S1).

Grid walk test revealed significantly increased forelimb faults. In vehicle-treated mice, the deficit was most severe 1 week after the lesion and persisted for at least 4 weeks ($p<0.05$ vs. baseline). In contrast, fasudil-treated mice did not show any deficits at 1 week or thereafter ($p<0.005$ vs. vehicle; two-way ANOVA for repeated measures), providing a behavioral correlate for the impaired RSFC (Figure 3).

The two L-NIO injections resulted in a single confluent lesion largely limited to the CC and elongated in the anteroposterior direction, when examined histologically at 1 month (Figure 4). Interestingly, despite worse initial loss of RSFC, lesion volumes were slightly smaller in the fasudil group compared with the vehicle at 1 month (0.095 vs. 0.1245 mm^3, respectively; $p=0.034$, t-test). The smaller lesion volumes in the fasudil arm stemmed from thinner lesions in the coronal plane rather than smaller lesions in the horizontal plane. To obtain some insight on the mechanisms, we further examined parallel coronal sections using immunohistochemistry for perilesional reactive astrocytosis (glial fibrillary acidic protein, GFAP), cortical synaptic density (synaptophysin) and corpus callosum mature oligodendrocyte density (glutathione S-transferase pi, GST-pi). We did not find a statistically significant difference between vehicle and fasudil arms with any of the markers (n=9 and 10, respectively; Figure 5).

DISCUSSION

This is the first demonstration of improved functional outcomes after a small and exclusively white matter lesion in the CC upon subacute systemic treatment with a ROCK inhibitor. Fasudil arm showed greater recovery of RSFC at 2 weeks as well as fewer forelimb faults that persisted at least 4 weeks.

We have recently shown that L-NIO causes significant and lasting hypoperfusion in cerebral cortex suggesting that CC lesions induced by L-NIO are ischemic strokes.[20] RhoA/ROCK inhibitors have been explored in ischemic stroke and the majority of studies suggested some benefit.[10] The isoform-nonselective ROCK inhibitor fasudil has also been tested in a small clinical trial in acute ischemic stroke initiated within the first 48 hours after stroke onset and continued twice a day for two weeks. Despite the rather delayed onset of treatment, fasudil improved the outcomes when measured at 2 weeks and one month using the modified Rankin Scale, as well as the motor deficits in Japanese Stroke Scale.[34] In our animal study, we also started fasudil in a rather delayed fashion and continued for 2 weeks, which yielded better recovery of function measured not only using the grid walk test but also an optical imaging approach. The latter is arguably a more sensitive functional indicator after a CC lesion than neurological deficits.[20,35]

Interestingly, we also found smaller lesions in the fasudil arm at 1 month, which could provide an explanation for better functional outcomes. However, given the fact that delayed onset (>6 hours) of treatment with ROCK inhibitors has not been effective in reducing the infarct volume in acute stroke,[36] it is unlikely that smaller lesions in the fasudil arm in our study reflect neuroprotection. Indeed, in one study using middle cerebral artery occlusion (MCAO) in rats, fasudil similarly improved the grid walk performance when started 1 day after and continued for 2 weeks, without affecting the infarct volume at 4 weeks.[37]

In another study, fasudil improved the grid walk performance when started 7 days after transient MCAO.[38] These data suggest that ROCK inhibition recruits mechanisms unrelated to neuroprotection to improve the long term recovery after an ischemic injury. Indeed, RhoA/ROCK inhibition augments neurogenesis and axonal regeneration after various forms of central nervous system injury,[10,16–19] including ischemic stroke.[38,39] Other potential mechanisms that might improve long-term outcomes and lead to smaller lesion volumes include decreased inflammation, BBB disruption and glial scar formation.[9]

Our study has limitations. First, the loss of connectivity on day 1 (i.e., prior to treatment onset) was slightly more severe in the fasudil arm compared with vehicle. We believe this is a random effect as the vehicle and treatment groups underwent identical procedures, and treatment onset took place after the completion of day 1 imaging. This contingency was exactly why we designed the study, *a priori*, for pre- vs. post-treatment comparisons within each study arm. Our interpretations of the efficacy of fasudil were based on this *a priori* statistical design. Nevertheless, day 14 connectivity appeared stronger in the fasudil arm compared with vehicle on the hemispheric maps (Figure 2B, upper panel). Therefore, we performed post-hoc exploratory analyses comparing day 14 interhemispheric connectivity directly between the vehicle and fasudil arms (Fisher's least significant difference test) and found higher connectivity 3-4 mm along the anteroposterior axis (data not shown), suggesting that despite a worse pre-treatment starting level, fasudil arm tended to have better connectivity on day 14. Second, we used only males since we did not intend to examine sexual dimorphism and aimed to avoid estrus cycle variations in this proof-of-concept study. Therefore, we do not know whether females would have benefited from fasudil to the same extent. Third, the intrinsic optical imaging of RSFC relies upon cerebral blood volume changes, and hence vasoreactivity reflecting neurovascular coupling. Therefore, vasomotor dysfunction or neurovascular uncoupling by L-NIO might ostensibly abolish intrinsic optical signal-based RSFC without affecting neuronal (i.e., electrical) connectivity. This is highly unlikely in our study because L-NIO injection and lesion were strictly limited to subcortical white matter whereas the intrinsic optical signal predominantly originates from relatively superficial cortex. Moreover, we performed imaging 24 hours after L-NIO injection, and RSFC was diminished far beyond the spatial extent of the lesion.

We designed this translational study to establish efficacy rather than the mechanisms. Given the pleiotropic nature of ROCK as a therapeutic target,[9] there are many potential mechanisms by which ROCK inhibition may contribute to improved outcomes in white matter injury. We quantified perilesional reactive astrocytosis, cortical synaptic density and corpus callosum mature oligodendrocyte density using immunohistochemistry but did not find a difference between the vehicle and fasudil arms at 1 month when fasudil efficacy still manifested as reduced foot faults. Future work will be directed towards elucidating the mechanisms of neurological improvement upon relatively delayed ROCK inhibition after a CC lesion and determine whether they overlap with previously demonstrated effects in other forms of central nervous system injury, such as reduced inflammation, BBB disruption, and glial scar formation, and enhanced axonal sprouting, neurogenesis, and remyelination. Given that fasudil is already in clinical use in the Far East,[40] clinical translation of our findings might be swift, if confirmed independently.

Supplementary Material

Refer to Web version on PubMed Central for supplementary material.

SOURCES OF FUNDING

National Institutes of Health (P01NS055104 to CA), Turkish Fulbright Commission (to SA).

NON-STANDARD ABBREVIATIONS AND ACRONYMS

DAPI	4′,6-diamidino-2-phenylindole
GFAP	glial fibrillary acidic protein
GST-pi	glutathione S-transferase pi
L-NIO	N^5-(1-Iminoethyl)-L-ornithine dihydrochloride
PBS	phosphate-buffered saline
ROCK	rho-associated kinase
RSFC	resting state functional connectivity

REFERENCES

1. Bailey EL, Smith C, Sudlow CL, Wardlaw JM. Pathology of lacunar ischemic stroke in humans--a systematic review. Brain Pathol. 2012;22:583–591. doi: 10.1111/j.1750-3639.2012.00575.x [PubMed: 22329603]
2. DeCarli C, Fletcher E, Ramey V, Harvey D, Jagust WJ. Anatomical mapping of white matter hyperintensities (WMH): exploring the relationships between periventricular WMH, deep WMH, and total WMH burden. Stroke. 2005;36:50–55. doi: 10.1161/01.STR.0000150668.58689.f2 [PubMed: 15576652]
3. Su E, Bell M. Diffuse Axonal Injury. Laskowitz D, Grant G, eds. In: Translational Research in Traumatic Brain Injury. 2016.
4. van der Knaap LJ, van der Ham IJ. How does the corpus callosum mediate interhemispheric transfer? A review. Behav Brain Res. 2011;223:211–221. doi: 10.1016/j.bbr.2011.04.018 [PubMed: 21530590]
5. Wardlaw JM, Valdes Hernandez MC, Munoz-Maniega S. What are white matter hyperintensities made of? Relevance to vascular cognitive impairment. Journal of the American Heart Association. 2015;4:001140. doi: 10.1161/JAHA.114.001140 [PubMed: 26104658]
6. Potter GM, Marlborough FJ, Wardlaw JM. Wide variation in definition, detection, and description of lacunar lesions on imaging. Stroke. 2011;42:359–366. doi: 10.1161/strokeaha.110.594754 [PubMed: 21193752]
7. Vermeer SE, Longstreth WT Jr., Koudstaal PJ. Silent brain infarcts: a systematic review. Lancet Neurol. 2007;6:611–619. doi: 10.1016/s1474-4422(07)70170-9 [PubMed: 17582361]
8. Leuchter AF, Dunkin JJ, Lufkin RB, Anzai Y, Cook IA, Newton TF. Effect of white matter disease on functional connections in the aging brain. J Neurol Neurosurg Psychiatry. 1994;57:1347–1354. doi: 10.1136/jnnp.57.11.1347 [PubMed: 7964810]
9. Shin HK, Salomone S, Ayata C. Targeting cerebrovascular Rho-kinase in stroke. Expert opinion on therapeutic targets. 2008;12:1547–1564. doi: [PubMed: 19007322]
10. Vesterinen HM, Currie GL, Carter S, Mee S, Watzlawick R, Egan KJ, Macleod MR, Sena ES. Systematic review and stratified meta-analysis of the efficacy of RhoA and Rho kinase inhibitors

in animal models of ischaemic stroke. Syst Rev. 2013;2:33. doi: 10.1186/2046-4053-2-33 [PubMed: 23687965]

11. Bito H, Furuyashiki T, Ishihara H, Shibasaki Y, Ohashi K, Mizuno K, Maekawa M, Ishizaki T, Narumiya S. A critical role for a Rho-associated kinase, p160ROCK, in determining axon outgrowth in mammalian CNS neurons. Neuron. 2000;26:431–441. doi: [PubMed: 10839361]
12. Lehmann M, Fournier A, Selles-Navarro I, Dergham P, Sebok A, Leclerc N, Tigyi G, McKerracher L. Inactivation of Rho signaling pathway promotes CNS axon regeneration. J Neurosci. 1999;19:7537–7547. doi: [PubMed: 10460260]
13. Sun X, Minohara M, Kikuchi H, Ishizu T, Tanaka M, Piao H, Osoegawa M, Ohyagi Y, Shimokawa H, Kira J. The selective Rho-kinase inhibitor Fasudil is protective and therapeutic in experimental autoimmune encephalomyelitis. J Neuroimmunol. 2006;180:126–134. doi: [PubMed: 16996142]
14. Baer AS, Syed YA, Kang SU, Mitteregger D, Vig R, Ffrench-Constant C, Franklin RJ, Altmann F, Lubec G, Kotter MR. Myelin-mediated inhibition of oligodendrocyte precursor differentiation can be overcome by pharmacological modulation of Fyn-RhoA and protein kinase C signalling. Brain. 2009;132:465–481. doi: 10.1093/brain/awn334 [PubMed: 19208690]
15. Paintlia AS, Paintlia MK, Singh AK, Singh I. Inhibition of rho family functions by lovastatin promotes myelin repair in ameliorating experimental autoimmune encephalomyelitis. Mol Pharmacol. 2008;73:1381–1393. doi: 10.1124/mol.107.044230 [PubMed: 18239032]
16. Mulherkar S, Tolias KF. RhoA-ROCK Signaling as a Therapeutic Target in Traumatic Brain Injury. Cells. 2020;9. doi: 10.3390/cells9010245
17. Watzlawick R, Sena ES, Dirnagl U, Brommer B, Kopp MA, Macleod MR, Howells DW, Schwab JM. Effect and reporting bias of RhoA/ROCK-blockade intervention on locomotor recovery after spinal cord injury: a systematic review and meta-analysis. JAMA Neurol. 2014;71:91–99. doi: 10.1001/jamaneurol.2013.4684 [PubMed: 24297045]
18. Forgione N, Fehlings MG. Rho-ROCK inhibition in the treatment of spinal cord injury. World neurosurgery. 2014;82:e535–539. doi: 10.1016/j.wneu.2013.01.009 [PubMed: 23298675]
19. Lemmens R, Jaspers T, Robberecht W, Thijs VN. Modifying expression of EphA4 and its downstream targets improves functional recovery after stroke. Hum Mol Genet. 2013;22:2214–2220. doi: 10.1093/hmg/ddt073 [PubMed: 23418304]
20. Aykan SA, Xie H, Lai JH, Zheng Y, Chung DY, Kura S, Anzabi M, Sugimoto K, McAllister LM, Yaseen MA, et al. Focal Subcortical White Matter Lesions Disrupt Resting State Cortical Interhemispheric Functional Connectivity in Mice. Cereb Cortex. 2021. doi: 10.1093/cercor/bhab134
21. Bauer AQ, Kraft AW, Wright PW, Snyder AZ, Lee JM, Culver JP. Optical imaging of disrupted functional connectivity following ischemic stroke in mice. Neuroimage. 2014;99:388–401. doi: 10.1016/j.neuroimage.2014.05.051 [PubMed: 24862071]
22. Chung DY, Oka F, Jin G, Harriott A, Kura S, Aykan S, Qin T, Edmiston WJ, Lee H, Yaseen MA, et al. Subarachnoid hemorrhage leads to early and persistent functional connectivity and behavioral changes in mice. bioRxiv. 2019:826891. doi: 10.1101/826891
23. Xie H, Chung DY, Kura S, Sugimoto K, Aykan SA, Wu Y, Sakadzic S, Yaseen MA, Boas DA, Ayata C. Differential effects of anesthetics on resting state functional connectivity in the mouse. J Cereb Blood Flow Metab. 2019:271678X19847123. doi: 10.1177/0271678X19847123
24. Bauer AQ, Kraft AW, Baxter GA, Wright PW, Reisman MD, Bice AR, Park JJ, Bruchas MR, Snyder AZ, Lee JM, et al. Effective Connectivity Measured Using Optogenetically Evoked Hemodynamic Signals Exhibits Topography Distinct from Resting State Functional Connectivity in the Mouse. Cereb Cortex. 2018;28:370–386. doi: 10.1093/cercor/bhx298 [PubMed: 29136125]
25. Kura S, Xie H, Fu B, Ayata C, Boas DA, Sakadzic S. Intrinsic optical signal imaging of the blood volume changes is sufficient for mapping the resting state functional connectivity in the rodent cortex. Journal of neural engineering. 2018. doi: 10.1088/1741-2552/aaafe4
26. Hakon J, Quattromani MJ, Sjolund C, Tomasevic G, Carey L, Lee JM, Ruscher K, Wieloch T, Bauer AQ. Multisensory stimulation improves functional recovery and resting-state functional connectivity in the mouse brain after stroke. Neuroimage Clin. 2018;17:717–730. doi: 10.1016/j.nicl.2017.11.022 [PubMed: 29264113]

27. Kura S, Xie H, Fu B, Ayata C, Boas DA, Sakadzic S. Intrinsic optical signal imaging of the blood volume changes is sufficient for mapping the resting state functional connectivity in the rodent cortex. Journal of neural engineering. 2018;15:035003. doi: 10.1088/1741-2552/aaafe4 [PubMed: 29451130]
28. White BR, Bauer AQ, Snyder AZ, Schlaggar BL, Lee JM, Culver JP. Imaging of functional connectivity in the mouse brain. PLoS ONE. 2011;6:e16322. doi: 10.1371/journal.pone.0016322 [PubMed: 21283729]
29. Paxinos G The mouse brain in stereotaxic coordinates. Academic; 2001.
30. Blasi F, Wei Y, Balkaya M, Tikka S, Mandeville JB, Waeber C, Ayata C, Moskowitz MA. Recognition memory impairments after subcortical white matter stroke in mice. Stroke. 2014;45:1468–1473. doi: 10.1161/STROKEAHA.114.005324 [PubMed: 24723319]
31. Aykan SA, Xie H, Lai JH, Zheng Y, Chung DY, Kura S, Anzabi M, Sugimoto K, McAllister LM, Yaseen MA, et al. Focal Subcortical White Matter Lesions Disrupt Resting State Cortical Interhemispheric Functional Connectivity in Mice. Cereb Cortex. 2021;31:4958–4969. doi: 10.1093/cercor/bhab134 [PubMed: 34037216]
32. Blasi F, Whalen MJ, Ayata C. Lasting pure-motor deficits after focal posterior internal capsule white-matter infarcts in rats. J Cereb Blood Flow Metab. 2015. doi: 10.1038/jcbfm.2015.7
33. Uchida H, Niizuma K, Kushida Y, Wakao S, Tominaga T, Borlongan CV, Dezawa M. Human Muse Cells Reconstruct Neuronal Circuitry in Subacute Lacunar Stroke Model. Stroke. 2017;48:428–435. doi: 10.1161/STROKEAHA.116.014950 [PubMed: 27999136]
34. Shibuya M, Hirai S, Seto M, Satoh S-i, Ohtomo E. Effects of fasudil in acute ischemic stroke: Results of a prospective placebo-controlled double-blind trial. Journal of the neurological sciences. 2005;238:31–39. doi: 10.1016/j.jns.2005.06.003 [PubMed: 16005902]
35. Rehme AK, Volz LJ, Feis DL, Eickhoff SB, Fink GR, Grefkes C. Individual prediction of chronic motor outcome in the acute post-stroke stage: Behavioral parameters versus functional imaging. Human brain mapping. 2015;36:4553–4565. doi: 10.1002/hbm.22936 [PubMed: 26381168]
36. Lee JH, Zheng Y, von Bornstadt D, Wei Y, Balcioglu A, Daneshmand A, Yalcin N, Yu E, Herisson F, Atalay YB, et al. Selective ROCK2 Inhibition In Focal Cerebral Ischemia. Annals of clinical and translational neurology. 2014;1:2–14. doi: 10.1002/acn3.19 [PubMed: 24466563]
37. Liu Y-h, Zhao Y, Huang F-z, Chen Y-h, Wang H-x, Bonney E, Liu B-q. Combination of early constraint-induced movement therapy and fasudil enhances motor recovery after ischemic stroke in rats. International Journal of Neuroscience. 2016;126:168–173. doi: [PubMed: 25526355]
38. Zhai ZY, Feng J. Constraint-induced movement therapy enhances angiogenesis and neurogenesis after cerebral ischemia/reperfusion. Neural Regen Res. 2019;14:1743–1754. doi: 10.4103/1673-5374.257528 [PubMed: 31169192]
39. Zhu YT, Zhang Q, Xie HY, Yu KW, Xu GJ, Li SY, Wu Y. Environmental enrichment combined with fasudil promotes motor function recovery and axonal regeneration after stroke. Neural Regen Res. 2021;16:2512–2520. doi: 10.4103/1673-5374.313048 [PubMed: 33907042]
40. Shirao S, Yoneda H, Ishihara H, Kajiwara K, Suzuki M. A proposed definition of symptomatic vasospasm based on treatment of cerebral vasospasm after subarachnoid hemorrhage in Japan: Consensus 2009, a project of the 25 Spasm Symposium. Surgical neurology international. 2011;2:74–74. doi: 10.4103/2152-7806.81968 [PubMed: 21748027]

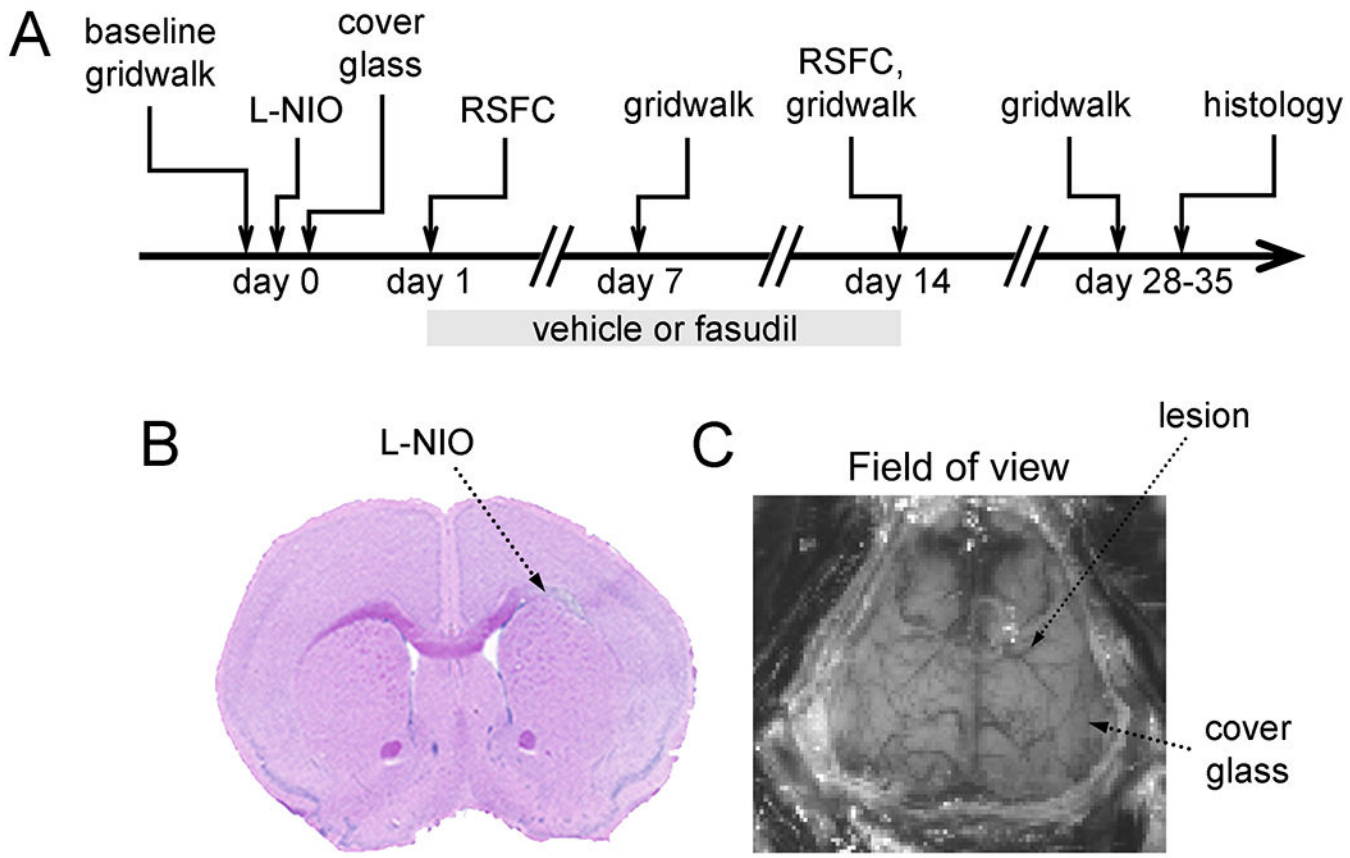

Figure 1: Experimental timeline and protocol.

(A) Experimental timeline showing the timing of assessments and interventions. (B) A representative hematoxylin/eosin-stained coronal section showing the angle and location of L-NIO injection (arrow) and resulting corpus callosum lesion at day 35. (C) Dorsal field of view of the cranial window as well as the RSFC images. Intact skull transparency was achieved by a chronic cover glass preparation. The approximate location of the L-NIO lesion is also shown.

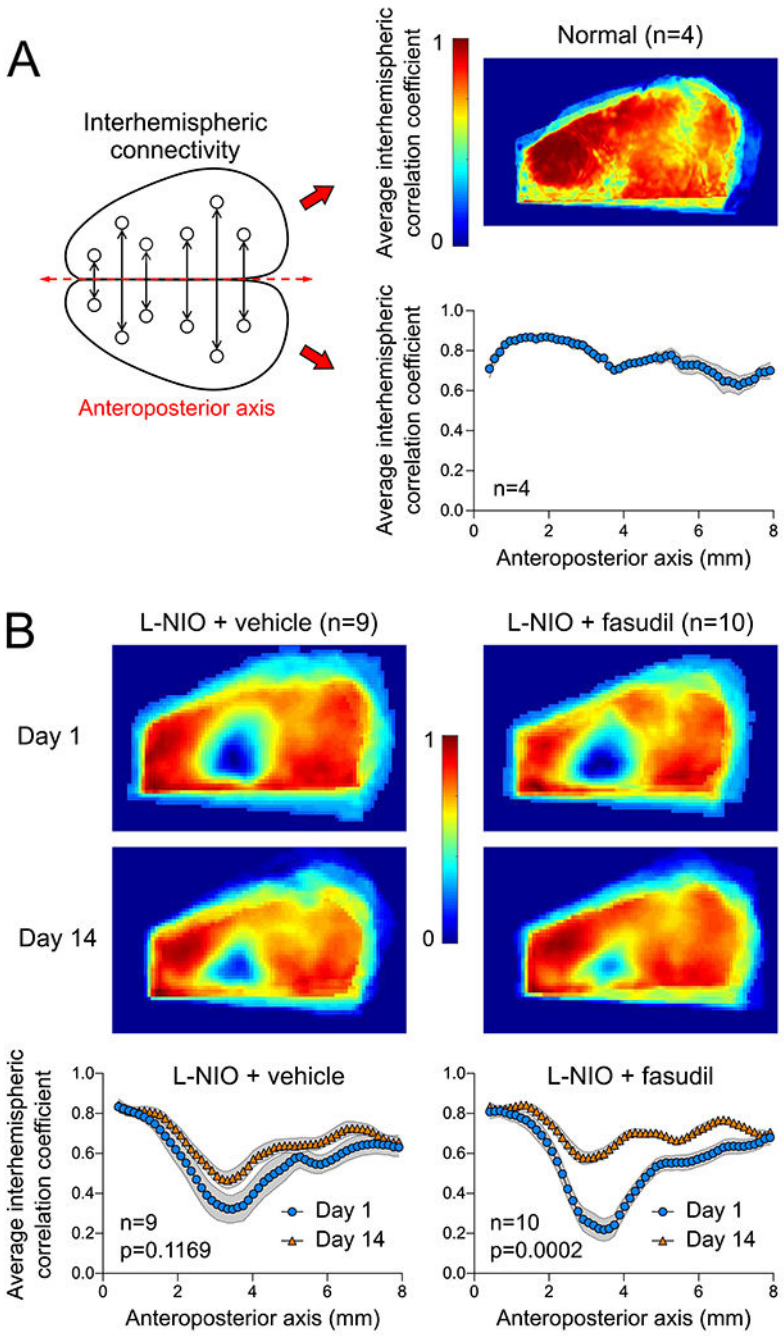

Figure 2: Interhemispheric homotopic resting state functional connectivity.

(A) Diagram of interhemispheric homotopic connectivity analysis using mirror pixels (left), the average interhemispheric homotopic connectivity map (right upper), and average interhemispheric homotopic correlation coefficients between mirror pixels averaged across the mediolateral axis and plotted along the anteroposterior axis, in mice with skull preparation only (i.e., no lesion). (B) Average interhemispheric homotopic connectivity maps (upper), and average interhemispheric homotopic correlation coefficients between mirror pixels plotted along the anteroposterior axis (lower) 1 or 14 days after L-NIO

injection in vehicle- or fasudil-treated mice. Day 1 and 14 imaging was performed in the same cohort. Two-way ANOVA for repeated measures on Fisher z-transformed data.

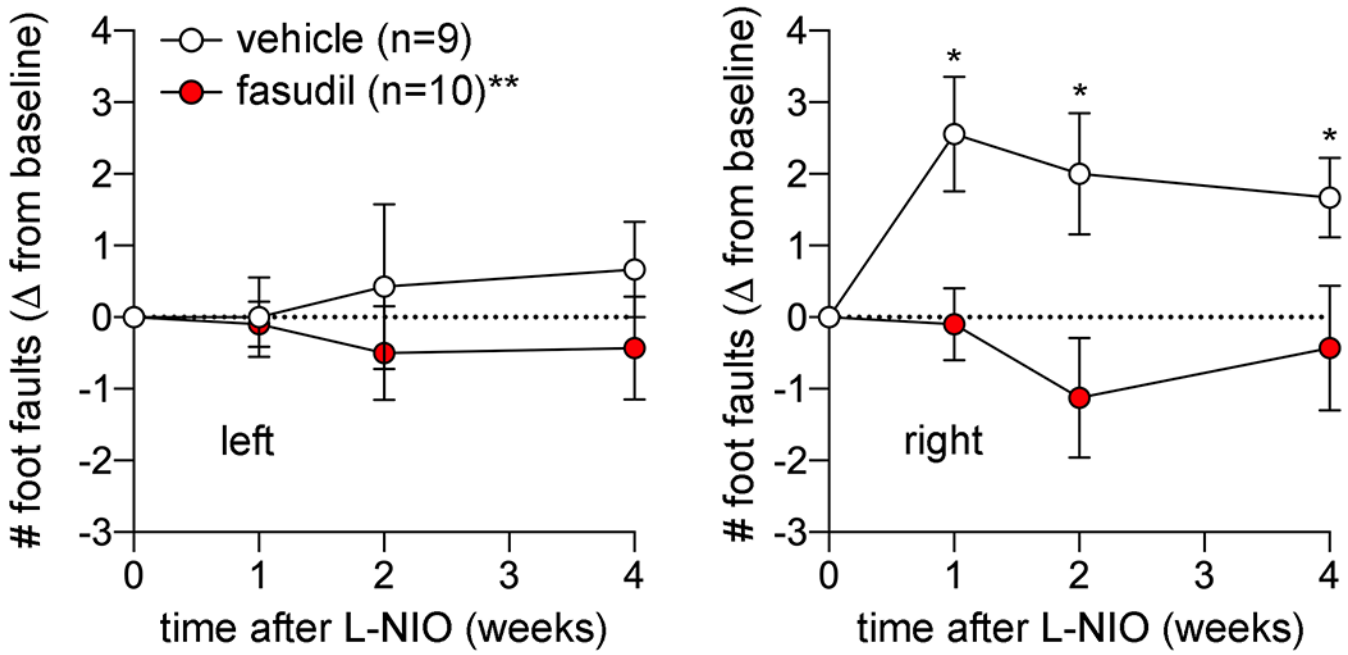

Figure 3: Neurological deficits.

Grid walk test to examine motor coordination in vehicle and fasudil treated groups longitudinally at baseline and 1,2 and 4 weeks after L-NIO injection. Data (mean ± standard error) are shown as change from baseline for right and left forelimb separately. Two-way ANOVA for repeated measures.

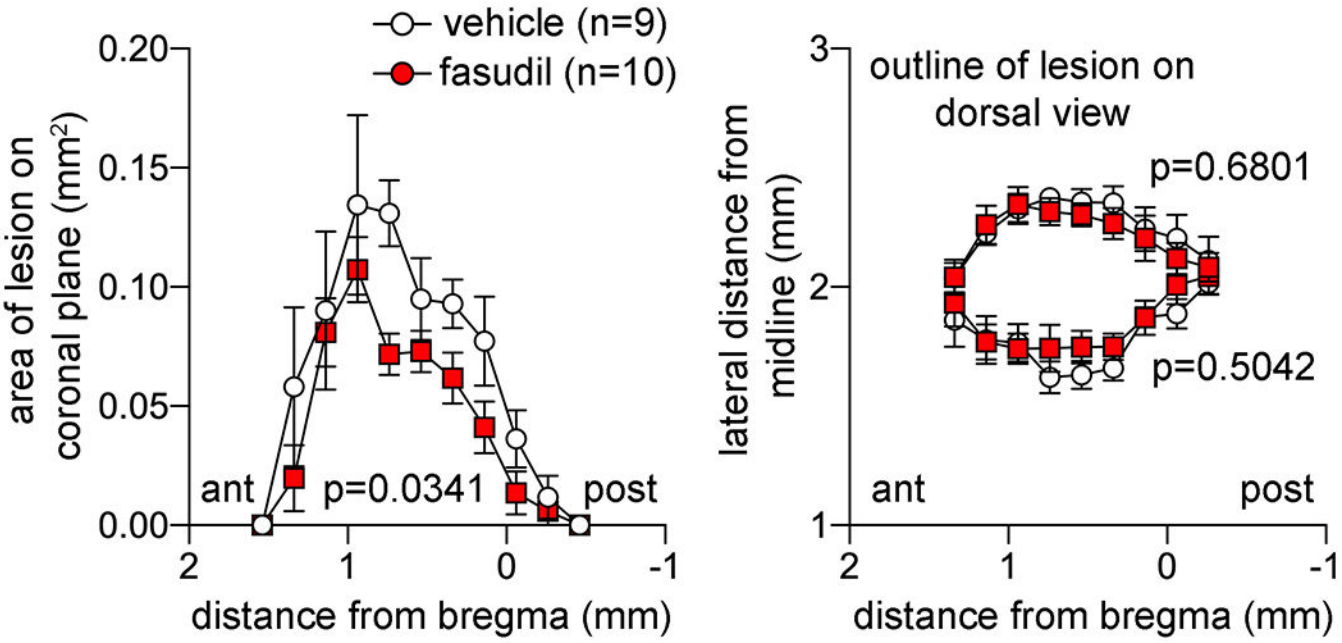

Figure 4: Lesion morphometry.

Lesion areas on coronal plane (left) and distance from the midline of the medial and lateral lesion boundaries at 1 month are plotted along the anteroposterior axis. Two-way ANOVA for repeated measures.

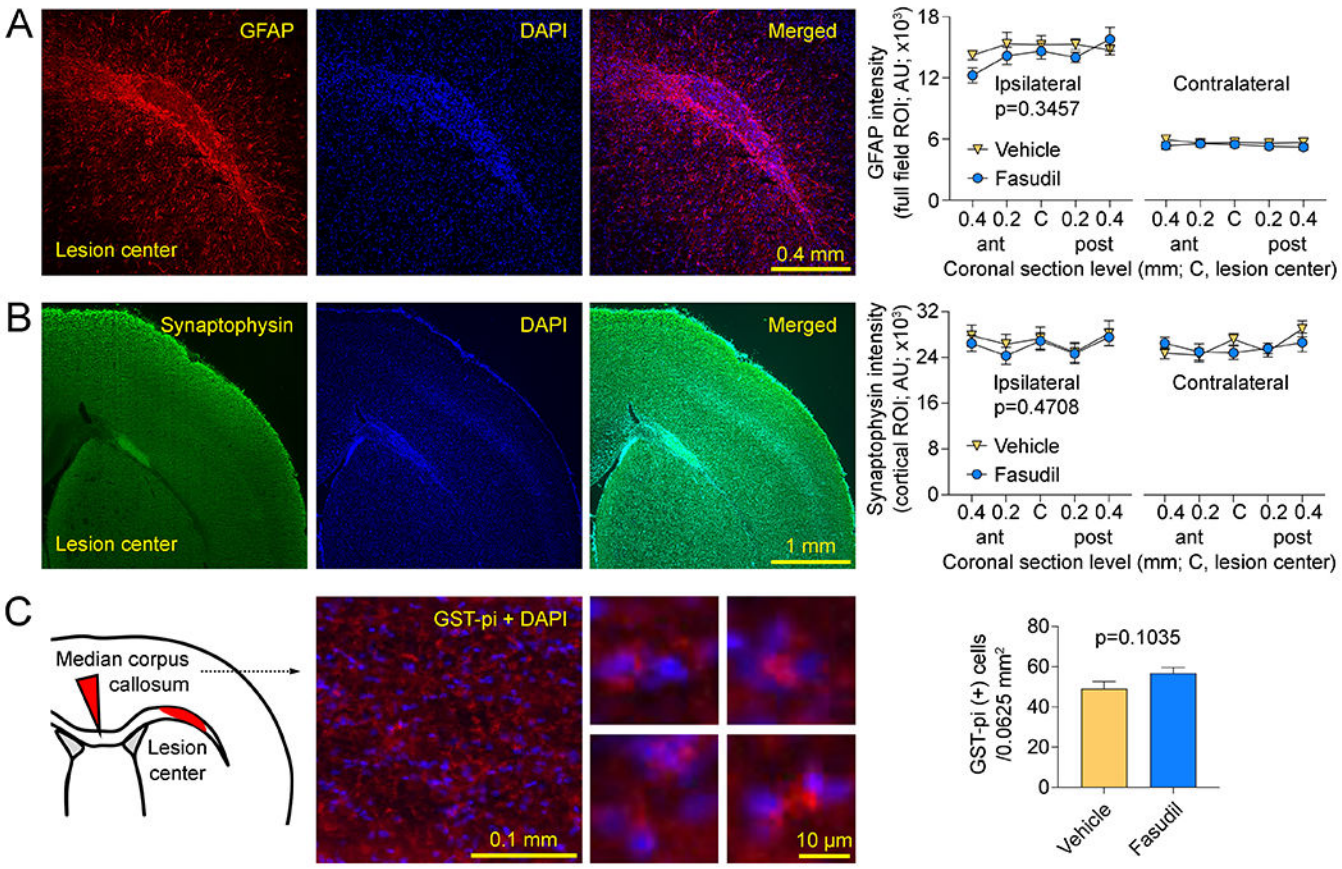

Figure 5: Immunohistochemical examination.

(A) Left: Representative sections show perilesional reactive astrocytosis (GFAP), nuclear stain DAPI and the merged image obtained at the coronal section in the center of the lesion along the anteroposterior axis. Right: GFAP intensity was quantified in the entire field of view positioned as shown, at 5 coronal section levels at 200 µm intervals centered along the anteroposterior axis of the lesion bilaterally (two-way ANOVA for repeated measures). (B) Left: Representative sections show synaptophysin, nuclear stain DAPI and the merged image obtained at the coronal section in the center of the lesion along the anteroposterior axis. The bright synaptophysin signal in the lesion represented autofluorescence and was excluded from the cortical region of interest. Right: Synaptophysin intensity was quantified in a region of interest outlining the entire cortex within the field of view positioned as shown, at 5 coronal section levels at 200 µm intervals centered along the anteroposterior axis of the lesion bilaterally (two-way ANOVA for repeated measures). (C) Left: Representative sections show merged images of mature oligodendrocytes (GST-pi) and nuclear stain DAPI from the median corpus callosum as shown in the inset. Higher magnification images show examples of GST-pi positive cells. Right: GST-pi positive cells were manually counted in the entire field positioned in the center of the median corpus callosum as shown in the inset (0.0625 mm^2) and centered along the anteroposterior axis of the lesion. All images were acquired using identical optical settings for a given marker and analyzed in a blinded fashion. P-values indicate vehicle vs. fasudil.